Incorporating Born solvation energy into the three-dimensional Poisson-Nernst-Planck model to study ion selectivity in KcsA K^+ channels

Xuejiao Liu and Benzhuo Lu*

State Key Laboratory of Scientific and Engineering Computing, National Center for Mathematics and Interdisciplinary Sciences, Academy of Mathematics and Systems Science, Chinese Academy of Sciences, Beijing 100190, China and School of Mathematical Sciences, University of Chinese Academy of Sciences, Beijing 100049, China

(Received 20 August 2017; published 26 December 2017)

Potassium channels are much more permeable to potassium than sodium ions, although potassium ions are larger and both carry the same positive charge. This puzzle cannot be solved based on the traditional Poisson-Nernst-Planck (PNP) theory of electrodiffusion because the PNP model treats all ions as point charges, does not incorporate ion size information, and therefore cannot discriminate potassium from sodium ions. The PNP model can qualitatively capture some macroscopic properties of certain channel systems such as current-voltage characteristics, conductance rectification, and inverse membrane potential. However, the traditional PNP model is a continuum mean-field model and has no or underestimates the discrete ion effects, in particular the ion solvation or self-energy (which can be described by Born model). It is known that the dehydration effect (closely related to ion size) is crucial to selective permeation in potassium channels. Therefore, we incorporated Born solvation energy into the PNP model to account for ion hydration and dehydration effects when passing through inhomogeneous dielectric channel environments. A variational approach was adopted to derive a Born-energy-modified PNP (BPNP) model. The model was applied to study a cylindrical nanopore and a realistic KcsA channel, and three-dimensional finite element simulations were performed. The BPNP model can distinguish different ion species by ion radius and predict selectivity for K^+ over Na^+ in KcsA channels. Furthermore, ion current rectification in the KcsA channel was observed by both the PNP and BPNP models. The I-V curve of the BPNP model for the KcsA channel indicated an inward rectifier effect for K^+ (rectification ratio of $\sim 3/2$) but indicated an outward rectifier effect for Na^+ (rectification ratio of $\sim 1/6$).

DOI: 10.1103/PhysRevE.96.062416

I. INTRODUCTION

Ion channels are important for facilitating the diffusion and transport of ions across cell membranes, and ion selectivity is crucial to many electrochemical and biomolecular systems [1–9], such as the transport of specific ion species through biomolecular channels [1,2,7,10]. The mechanism of selective ion transport in potassium channels has been widely studied in recent decades [2,11,12]. A longstanding question is why larger K^+ ions are selected over smaller Na^+ ions. Various theoretical methods have been employed to study the thermodynamic and kinetic basis for the selective permeation of ions through different channels, including molecular dynamics (MD) [2,13–16], Brownian dynamics (BD) [17–20], and Monte Carlo (MC) [1,17,21,22], and Poisson-Nernst-Planck (PNP) simulations [23–27]. The former three methods are particle simulations that can capture discrete particle effects and microscopic dynamics. In contrast, the PNP model is a continuum model that can capture macroscopic transport properties, but it describes particle interactions less accurately. The PNP model is based on the mean-field approximation of an ionic solution, in which ions are considered to be point charges continuously distributed in solution. In the PNP model, electrostatic potential is calculated through the Poisson equation, and ion concentrations and currents are calculated with the Nernst-Planck equation. PNP calculations use much less computational power relative to other methods, and the results, such as current-voltage characteristics (I-V curve), can be directly compared with experimental data. However, as PNP theory neglects discrete particle effects and ionic specificity, it cannot distinguish K^+ from Na^+ and, hence, the traditionally used PNP model is not suitable for studying the selectivity of potassium channels.

A number of previous investigations have indicated that ion selectivity by micropores is mostly determined by size effects (and the relevant dehydration effect) as well as electrostatic interactions [5,28–31]. In the interaction energy point of view, the size "matching" can be attributed to a lower energy barrier when passing the channel. This process is closely related to the ion solvation (hydration) and desolvation (dehydration) processes, which was also mentioned many times in the literature [32–35]. Recently, several improved PNP models have been proposed based on incorporation of ion steric effects [27,36–38]. However, to our knowledge and experience, it is difficult for these size-modified models to predict the distinct selectivity for potassium over sodium in realistic KcsA channels [31,38]. It is recognized that size-dependent ion dehydration plays an important role in the selective transport of ions in KcsA channels (see the following figure and discussion). As far as we know, there is no existing PNP model that explicitly takes ion hydration interactions into account.

Ion hydration and dehydration are associated with free energy change when transferring from the solvent region (high dielectric) to the channel region (low dielectric). Born energy [39] [Eq. (1)], defined as the electrostatic energy required to transfer an ion from a vacuum with the dielectric constant ϵ_0 to a medium with the dielectric constant ϵ, is a good approximation of ion hydration energy:

$$G_{\text{Born}} = \frac{q^2}{2a}\left(\frac{1}{\epsilon} - \frac{1}{\epsilon_0}\right), \tag{1}$$

*bzlu@lsec.cc.ac.cn

where $q = Ze$ (Z is the valence of the ion and e is the elementary charge) and a is the radius of the ion. The Born model assumes that the dielectric medium (ϵ) is homogenous. However, because ion hydration is largely governed by the interaction between the ion and the nearby solvent molecules, in smoothly inhomogeneous medium (ϵ varies smoothly with position, as in this study where the diffusive domain is mainly divided in two constant ϵ regions, the bulk high-ϵ_s region and the low-ϵ_c pore region) we still use the Born model [with a position-dependent $\epsilon(r)$] to approximate the free energy change at different positions. Boda *et al.* developed an interpolation method using the induced charge computation method for treating the passage of a charged hard sphere ion as it passes through a sharp dielectric boundary. They analyzed the various energy terms using a spherical ion passing through an infinite flat dielectric boundary [40]. They also used grand canonical Monte Carlo simulation to study the effect of solvation energy on monovalent vs divalent ion selectivity in a reduced model of the L-type calcium channel. In that method, they found that changing the dielectric coefficient in the channel does not produce observed change in selectivity, and claimed that it is because the larger solvation penalty is counterbalanced by the enhanced Coulomb attraction inside the channel [41]. However, for general ion channel geometry, the dielectric transition region is much more irregular (such as the entrance of the KcsA channel in this work), and a sharp dielectric interface is an ideal approximation, so a diffuse interface would be more realistic. In these cases, the above induced charge calculation is intractable. The current PNP model numerically solves the Poisson equation to strictly determine the systems' electrostatic interaction (at the mean field level) with arbitrary geometry and inhomogenous dielectric media. However, this continuum description does not capture well the discrete particle effect such as the prominent ion solvation effect as in above mentioned Monte Carlo method. In this work, we incorporate the Born solvation energy into the PNP model. If we treat the dielectric coefficient ϵ as position dependent, the Born solvation energy can be evaluated analytically and locally, and its variation during passage across a membrane channel reflects hydration and dehydration processes. This indicates that the permeability of a channel to ions depends on the ionic radius and on the dielectric constant of the channel and membrane [42,43]. Figure 1 illustrates the change in Born solvation energy for an ion moving from left (high dielectric region) to right (low dielectric region). As shown in Fig. 1, the Born solvation energy increases when a point charge moves from a high dielectric region to a low dielectric region. The potential barrier can be calculated as

$$\Delta G_{\text{Born}} = \frac{q^2}{2a}\left(\frac{1}{\epsilon_m} - \frac{1}{\epsilon_s}\right). \tag{2}$$

Born energy is a type of strong interaction between an individual ion and surrounding solvent molecules, and we can therefore also refer to it as Born self-energy. As mentioned above, the mean-field continuum PNP model is based on average interactions and neglects discrete particle effects, which can cause underestimation of the Born energy of individual ions. In this work, we incorporated the Born solvation energy equation into the traditional mean-field free energy form and used a variational approach to derive a Born-energy-modified PNP (BPNP) model. We applied this new model to KcsA channel and nanopore systems to demonstrate its predictive capability of the selective permeation of potassium ions.

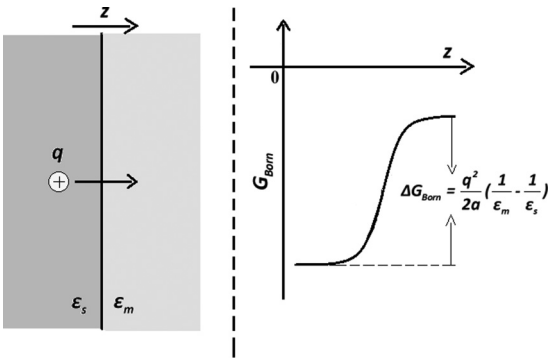

FIG. 1. Schematic and corresponding change in Born solvation energy for an ion moving from a high dielectric region (ϵ_s) to a low dielectric region (ϵ_m).

II. MODELS AND METHODS

A. Mean-field free energy with Born solvation energy

In our previous work [44], we presented a general and complete mean-field free energy functional by incorporating nonhomogeneous boundary effects in bounded domains. The major goal of the study was to create consistency among derived partial differential equation (PDE) models, the free energy functional, and nonhomogeneous Dirichlet-Neumann boundary conditions. The consistent generalized Poisson-Boltzmann (PB) and PNP equations can be derived from the new complete free energy functional using a variational approach. A typical modeling domain is illustrated in Fig. 2, and the free energy functional is as follows [44]:

$$\begin{aligned} F[c] = &\int_\Omega \frac{1}{2}\rho(c)\phi(c)\,dV \\ &+ \int_{\Gamma_N} \frac{1}{2}\sigma\phi(c)\,dS - \int_{\Gamma_D} \frac{1}{2}\epsilon(r)\frac{\partial\phi}{\partial n}\phi_0\,dS \\ &+ \beta^{-1}\sum_{i=1}^{K}\int_\Omega c_i[\ln(\Lambda^3 c_i) - 1]\,dV - \sum_{i=1}^{K}\int_\Omega \mu_i c_i\,dV. \end{aligned} \tag{3}$$

Here, ρ is the total charge density, defined as

$$\rho = \rho^f + \sum_{i=1}^{K} q_i c_i, \tag{4}$$

where $q_i = Z_i e$ (Z_i is the valence of the ith ionic species and e is the elementary charge); K is the number of diffusive ion species in solution that are considered in the system; ρ^f is the permanent (fixed) charge distribution,

$$\rho^f(x) = \sum_j q_j \delta(x - x_j),$$

which is an ensemble of singular charges q_j located at x_j inside biomolecules; $\beta^{-1} = k_B T$ (k_B is the Boltzmann constant and

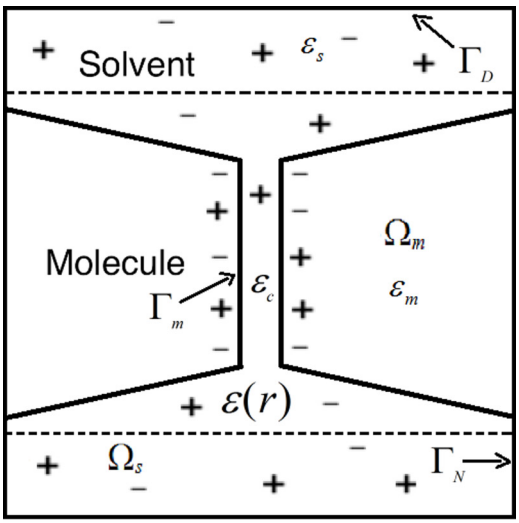

(a)

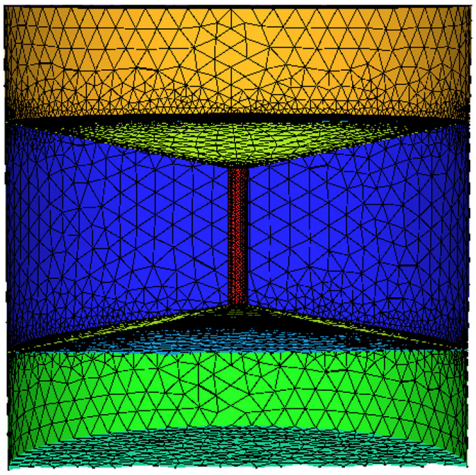

(b)

FIG. 2. The (a) geometry and (b) mesh of the cylindrical nanopore.

T is the temperature); Λ is the thermal de Broglie wavelength; μ_i is the chemical potential of the ith ionic species; $\phi = \phi(c)$ is the electrostatic potential, where $c = (c_1, \ldots, c_K)$, and ϕ is determined by the Poisson equation [Eq. (5)] [ϵ can be either position or ion concentration dependent; in this study, we only consider the position-dependent case $\epsilon(r)$]; and c_i is the concentration of the ith ionic species:

$$\begin{aligned} -\nabla \cdot (\epsilon(r)\nabla\phi(c)) &= \rho(c) \text{ in } \Omega, \\ \epsilon(r)\frac{\partial\phi}{\partial n} &= \sigma \text{ on } \Gamma_N, \\ \phi &= \phi_0(r) \text{ on } \Gamma_D. \end{aligned} \tag{5}$$

To overcome the inability of the PNP model to predict ion selectivity in ion channels and reduce overestimation of the shielding effect [19,20], as discussed in Sec. I, we considered ion self-energy changed when an ion passes through a continuous dielectric boundary and incorporated the Born-solvation-energy equation into the mean-field free energy equation. We assume that the ion has a finite radius to calculate the Born solvation energy despite the fact that we treat the ion as a point charge in the model. The total free energy including the Born solvation energy is represented as follows:

$$\begin{aligned} F[c] = &\int_\Omega \frac{1}{2}\rho(c)\phi(c)\,dV \\ &+ \int_{\Gamma_N} \frac{1}{2}\sigma\phi(c)\,dS - \int_{\Gamma_D} \frac{1}{2}\epsilon(r)\frac{\partial\phi}{\partial n}\phi_0\,dS \\ &+ \beta^{-1}\sum_{i=1}^{K}\int_\Omega c_i[\ln(\Lambda^3 c_i) - 1]\,dV - \sum_{i=1}^{K}\int_\Omega \mu_i c_i\,dV \\ &+ \sum_{i=1}^{K}\int_\Omega c_i\alpha\frac{q_i^2}{2a_i}\left(\frac{1}{\epsilon(r)} - \frac{1}{\epsilon_0}\right)dV, \end{aligned} \tag{6}$$

where a_i is the ion radius of the ith ionic species, and ϵ is the dielectric coefficient, which locally depends on the position of ions. Because the Born energy is a kind of specific electrostatic interaction (between individual ions and the surrounding solvent molecules), and the previous energy form already includes electrostatic interactions of the whole system in a mean-field level (but underestimates the strong specific solvation effect—there are even no explicit solvation terms in the energy form), incorporation of the Born solvation energy would cause certain overlap in electrostatic interactions. As the part of the overlap energy is hard to determine within current methodology, we introduced an adjustable parameter α to account for this overlap. In the next section, we begin with this free energy functional and apply a variational approach to derive the BPNP equations.

The above free energy (6) can also be reformulated into another form. The chemical potential μ_i can be evaluated by considering the special case of equilibrium state, i.e., $\frac{\delta F}{\delta c_i} = 0$, and we obtain

$$\mu_i = q_i\phi + \beta^{-1}\ln(\Lambda^3 c_i) + \alpha\frac{q_i^2}{2a_i}\left(\frac{1}{\epsilon(r)} - \frac{1}{\epsilon_0}\right). \tag{7}$$

Considering $r \to \infty$, the potential $\phi \to 0$, $\epsilon(r) \to \epsilon_s$, and defining $c_i \to c_i^b$ (denoting the bulk concentration of the ith species), we get

$$\mu_i = \beta^{-1}\ln\left(\Lambda^3 c_i^b\right) + \alpha\frac{q_i^2}{2a_i}\left(\frac{1}{\epsilon_s} - \frac{1}{\epsilon_0}\right). \tag{8}$$

Substituting Eq. (8) into Eq. (6), an alternative free energy form can be expressed as

$$\begin{aligned} F[c] = &\int_\Omega \frac{1}{2}\rho(c)\phi(c)\,dV \\ &+ \int_{\Gamma_N} \frac{1}{2}\sigma\phi(c)\,dS - \int_{\Gamma_D} \frac{1}{2}\epsilon(r)\frac{\partial\phi}{\partial n}\phi_0\,dS \\ &+ \beta^{-1}\sum_{i=1}^{K}\int_\Omega c_i\left[\ln\left(c_i/c_i^b\right) - 1\right]dV \\ &+ \sum_{i=1}^{K}\int_\Omega c_i\alpha\frac{q_i^2}{2a_i}\left(\frac{1}{\epsilon(r)} - \frac{1}{\epsilon_s}\right)dV. \end{aligned} \tag{9}$$

B. Born-energy-modified PNP equations

The ionic flux J_i is given by the following constitutive relationship:

$$J_i = -m_i c_i \nabla \mu_i, \tag{10}$$

where m_i is the ion mobility, which is related to the diffusivity D_i through the Einstein relation, $D_i = \beta^{-1} m_i$. Substituting Eq. (7) into Eq. (10), the transport equations are obtained from the mass and current conservation law:

$$\begin{aligned}\frac{\partial c_i}{\partial t} &= -\nabla \cdot J_i \\ &= \nabla \cdot \left(\beta D_i c_i \nabla \left\{ q_i \phi + \beta^{-1} \ln(\Lambda^3 c_i) \right.\right. \\ &\quad \left.\left. + \alpha \frac{q_i^2}{2a_i} \left(\frac{1}{\epsilon(r)} - \frac{1}{\epsilon_0} \right) \right\} \right).\end{aligned}$$

The complete BPNP equations take the form

$$-\nabla \cdot (\epsilon(r) \nabla \phi) = \rho^f + \sum_{i=1}^{K} q_i c_i \text{ in } \Omega, \tag{11}$$

$$\frac{\partial c_i}{\partial t} = \nabla \cdot \left\{ D_i \left[\nabla c_i + \beta c_i \nabla \left(q_i \phi + \alpha \frac{q_i^2}{2a_i} \left(\frac{1}{\epsilon(r)} - \frac{1}{\epsilon_0} \right) \right) \right] \right\}, \quad \times \text{ in } \Omega_s, \quad i = 1,2,\ldots,K, \tag{12}$$

$$\epsilon(r) \frac{\partial \phi}{\partial n} = \sigma \text{ on } \Gamma_N, \quad \phi = \phi_0(r) \text{ on } \Gamma_D,$$
$$c_i = c_i^b \text{ on } \Gamma_D, \quad J_i \cdot n = 0 \text{ on } \Gamma_m,$$

where n is the exterior unit normal. When the dielectric coefficient is a constant rather than position dependent, the above BPNP equations can be simplified to the traditional PNP equations.

To take into account the effect of Born solvation energy, we calculated the current inside the channel. In the BPNP model, electrical current can be calculated as

$$\begin{aligned}I_z = -\sum_i q_i \int_S D_i \left(\frac{\partial c_i}{\partial z} + \frac{q_i}{k_B T} c_i \frac{\partial \phi}{\partial z} \right. \\ \left. + \frac{1}{k_B T} c_i \alpha \frac{q_i^2}{2a_i} \frac{\partial \left(\frac{1}{\epsilon(r)} - \frac{1}{\epsilon_0} \right)}{\partial z} \right) dx\, dy,\end{aligned} \tag{13}$$

where S is a cut plane at any cross section inside the pore, and D_i is the diffusion coefficient of the ith ionic species. The bulk diffusion coefficients are $D_{\text{Na}}^{\text{bulk}} = 0.133$ Å^2/ps, $D_{\text{K}}^{\text{bulk}} = 0.196$ Å^2/ps, and $D_{\text{Cl}}^{\text{bulk}} = 0.203$ Å^2/ps for Na^+, K^+, and Cl^-, respectively. When the ions approach and enter the channel, a position-dependent diffusion coefficient is adopted similar to the form in Ref. [9]:

$$D_i(r) = D_i(z) = D_i^{\text{bulk}} \left(d_1 + \frac{1.0 - d_1}{1.0 + e^{-\frac{|z| - z_0}{\Delta z}}} \right), \tag{14}$$

where D_i^{bulk} is the bulk diffusion coefficient (as defined before), $d_1 = 0.1$ is the ratio of the effective diffusion coefficient in the channel to that in the bulk region, z_0 is the section for which $D_i(z_0) = \frac{1}{2}(D_i^{\text{bulk}} + d_1 D_i^{\text{bulk}})$, and Δz is a parameter for smoothing.

C. Generalized Boltzmann distributions

Based on the free energy functional (9), we can derive the generalized Boltzmann distributions in the equilibrium state. If $c = (c_1, \ldots, c_K)$ is in equilibrium, the electrostatic free energy $F = F(c)$ is minimized:

$$\begin{aligned}&\frac{\delta F[c]}{\delta c_i} = q_i \phi + \beta^{-1} \ln\left(c_i / c_i^b\right) + \alpha \frac{q_i^2}{2a_i} \left(\frac{1}{\epsilon(r)} - \frac{1}{\epsilon_s} \right) = 0, \\ &\Rightarrow \; c_i = c_i^b \exp\left\{ -\beta q_i \phi(c) - \frac{\alpha \beta q_i^2}{2a_i} \left(\frac{1}{\epsilon(r)} - \frac{1}{\epsilon_s} \right) \right\}, \\ &\qquad i = 1, \ldots, K,\end{aligned} \tag{15}$$

where $c_i \to c_i^b$, $\epsilon(r) \to \epsilon_s$, and $\phi \to 0$ as $r \to \infty$. We call Eqs. (15) the Born-energy-modified generalized Boltzmann distributions, as they generalize the classical Boltzmann distributions $c_i = c_i^b e^{-\beta q_i \phi}$ $(i = 1, \ldots, K)$ when $\alpha = 0$ (i.e., Born energy is not considered).

D. Position-dependent dielectric coefficient

Ionic solutions consist of charged ions, "hydration" solvent molecules near the vicinity of the ions, and "free" solvent molecules. The effective dielectric permittivity inside a channel is thought to be related to ionic hydration shells [45,46] or the dehydration state in many cases. Due to limitations of the channel structure, the effective dielectric coefficient around the ions inside the channel will decrease due to the removal of water. Moreover, many experiments and theoretical analyses have indicated that the dielectric coefficient decreases with increasing local ionic concentrations [47–49]. For simplicity in this work, we suppose a high dielectric constant outside the channel and a low dielectric constant inside the channel, and there is a narrow smooth transition region between them (see an example in Fig. 3). The position-dependent dielectric coefficient can take a form similar to Eq. (14):

$$\epsilon(r) = \epsilon(z) = \epsilon_s \left(a_1 + \frac{1.0 - a_1}{1.0 + e^{-\frac{|z| - z_0}{\Delta z}}} \right), \tag{16}$$

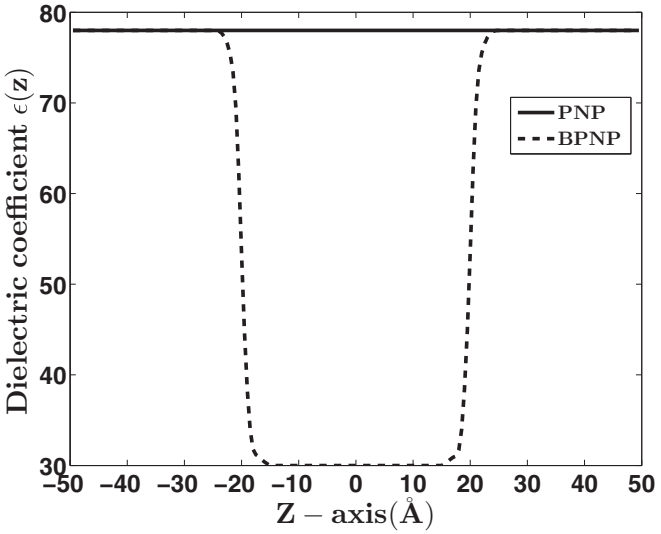

FIG. 3. Dielectric coefficient profiles for the PNP and BPNP models.

where ϵ_s is the bulk dielectric coefficient ($\epsilon_s = 78$), a_1 is the ratio of the effective dielectric coefficient in the channel (ϵ_c) to that in the bulk region, z_0 is the section for which $\epsilon(z_0) = \frac{1}{2}(\epsilon_s + \epsilon_c)$, and Δz is a parameter for smoothing. In Sec. III B, we give the clear and explicit expressions for the diffusion and dielectric coefficients.

In Sec. III, we use Eq. (16) as an example to test the effect of Born solvation energy in the BPNP system of Eqs. (11) and (12).

E. Numerical and software implementations

The three-dimensional (3D) BPNP equations were solved using the finite element method (FEM) [26,50,51], which is advantageous for modeling irregular geometries with complex boundary conditions. Our finite element algorithms were based on tetrahedral meshes. The volume mesh of a cylindrical nanopore was generated using COMSOL5.2, and the ion channel volume mesh was generated using our biomolecule surface meshing software TMSMESH [52] and a few other meshing tools. TMSMESH was used to generate a manifold surface mesh that can handle large systems. The program TETGEN [53] was employed to generate the tetrahedral volume mesh. The details are described in the next section. The algorithms were implemented with the 3D parallel adaptive finite element package PHG [54]. We adopted a decoupled iteration method to solve the coupled Poisson equation and Nernst-Planck (NP) equations. The under-relaxation scheme was employed to guarantee the convergence of the algorithms [51].

In the next section, we apply the system of Eqs. (11) and (12) to a cylindrical nanopore and a realistic potassium channel. In the cylindrical nanopore example, we only solve the BPNP model in the solvent region Ω_s and do not consider the molecular domain Ω_m.

III. RESULTS AND DISCUSSIONS

A. Simulations of a cylindrical nanopore

To evaluate the effect of Born solvation energy, we first applied the system of Eqs. (11) and (12) to a cylindrical nanopore. A cylindrical nanopore with a height of 30 Å and a pore radius of 2 Å was placed in the middle of a cubic box (100 Å × 100 Å × 100 Å). As shown in Fig. 6, the narrow radii of the selectivity filter in the KcsA channel is about 2 Å. In order to better compare the results of the nanopore and the KcsA channel, so we set the same pore radius, 2 Å, in the cylindrical nanopore simulation. To simulate a realistic ionic solution system, we set the charge density on the inner surface of the nanopore to -0.085 C/m^2. The boundary potential at the upper side of the box was fixed to zero, and that at the bottom side was set from -200 to 200 mV to obtain different membrane potential differences. The geometry and mesh of the cylindrical nanopore is illustrated in Fig. 2. To straightly study the selectivity of K^+ and Na^+, our modeled system is a ternary mixture of K^+, Na^+, and Cl^- in the electrolyte. The Born radii are used in this work, i.e., $a_K = 1.95$ Å, $a_{Na} = 1.62$ Å, and $a_{Cl} = 2.26$ Å for K^+, Na^+, and Cl^-, respectively. The Born radius is obtained by the free energy needed to bring the ion from vacuum into the electrolyte. In this respect, the Born radius can be considered an experimentally derived parameter

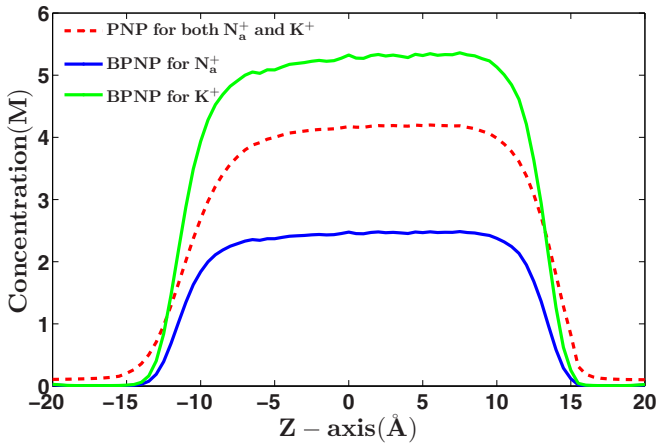

FIG. 4. Cation distributions based on PNP and BPNP models for a ternary electrolyte system (with Na^+, K^+, and Cl^- ion species) in a cylindrical nanopore under a fixed membrane voltage $V_0 = -0.20$ V and bulk concentration $c^b_{Na} = 0.1$ M, $c^b_K = 0.1$ M, and $c^b_{Cl} = 0.2$ M.

[41]. We tested some values of the parameter α in Eq. (6) (the details can be seen in Sec. III B) and set α to 0.10 as an example to show the results of the cylindrical nanopore in this section.

Figure 2(a) demonstrates a typical biophysical ion transport system. The domain Ω_s denotes the solvent region filled with ionic solution. The solute region Ω_m is the domain occupied by the membrane, channel protein, or nanopore [7,31,51,55,56]. The whole computational domain is denoted as $\Omega = \Omega_m \cup \Omega_s$. Domains Ω_m and Ω_s are separated by a molecular surface Γ_m. We used Γ_D and Γ_N to represent boundaries with Dirichlet and Neumann boundary conditions, respectively. The boundary of the solvent region is represented as $\Gamma_s = \Gamma_D \cup \Gamma_N$. The domain within the dotted lines is a variable dielectric region. The volume mesh of the cylindrical nanopore was generated with COMSOL5.2, as shown in Fig. 2. Figure 3 illustrates the profiles of the dielectric coefficients for the PNP (solid lines) and BPNP (dotted lines) models. As shown in Fig. 3, the position-dependent dielectric coefficient has a continuous change, as defined in Eq. (16).

Figure 4 shows the cation distributions based on the PNP and BPNP models in a cylindrical nanopore under a fixed membrane voltage ($V_0 = -0.20$ V) and bulk concentration ($c^b_{Na} = 0.1$ M, $c^b_K = 0.1$ M, and $c^b_{Cl} = 0.2$ M). As shown in Fig. 4, the BPNP model can distinguish between cations with the same charge but different ion radii. This result can be explained by analyzing the Born solvation energy. The Born solvation energy will increase when an ion moves from the solvent region to the channel. However, the potential barrier defined by Eq. (2) will decrease with increasing ion radius. Therefore, K^+ is more likely to occupy the channel.

Figure 5 shows the PNP and BPNP simulations of voltage-current (I-V) curves for cations in a cylindrical nanopore with three ion species ($c^b_{Na} = 0.1$ M, $c^b_K = 0.1$ M, and $c^b_{Cl} = 0.2$ M) under different membrane voltages from -200 to 200 mV. Due to the symmetric shape and surface charge distribution of the nanopore, the two models predict a symmetrical current under different membrane voltages. The difference of I-V curves for Na^+ and K^+ in the PNP model is only due to the

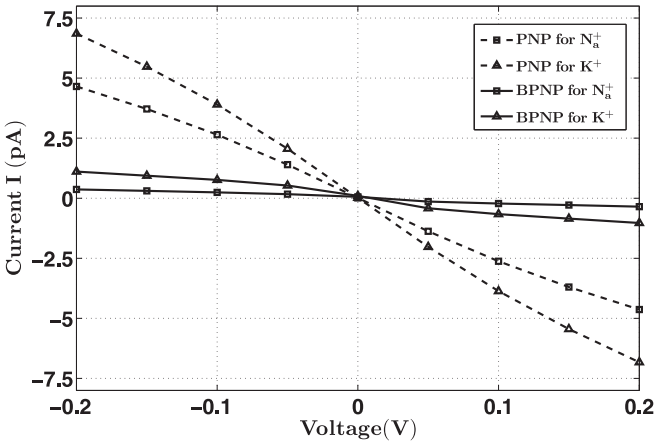

FIG. 5. I-V curves for cations based on the PNP and BPNP models in a cylindrical nanopore with three ions ($c^b_{\mathrm{Na}} = 0.1$ M, $c^b_{\mathrm{K}} = 0.1$ M, and $c^b_{\mathrm{Cl}} = 0.2$ M) under a change in membrane voltage from −200 to 200 mV.

different diffusion coefficient for Na^+ and K^+. The I-V curves based on the BPNP model indicate a distinct selectivity of K^+ over Na^+.

As previously discussed, the new BPNP model overcomes the shortcomings of the traditional PNP model for studying selectivity in ion channels. The BPNP model can distinguish cations with the same charge but different ion radii. In the next section, we use the BPNP model to investigate ion selectivity in a realistic potassium channel.

B. Simulations of a potassium channel

In this section, we investigate the application of the BPNP model [Eqs. (11) and (12)] to a realistic potassium channel: the bacterial channel KcsA [see Protein Data Bank (PDB) entry 1BL8]. The channel is constructed of 5892 atoms, with three primary sections: an opening pore on the cytoplasmic side of the cell interior, a large water-filled cavity, and a narrow selectivity filter. The narrow selectivity filter is only 12 Å long, whereas the remainder of the pore is wider [57]. Due to its relatively complete channel functions, the KcsA channel has been widely used to study ion selectivity. Figure 6(a) shows the molecular surface of the KcsA channel obtained using the software VMD 1.9.1 [58]. From bottom to top, we can clearly see the channel pores, water-filled cavity, and narrow selectivity filter with binding sites for cations. The radius of the KcsA channel was calculated based on molecular surface mesh according to the method described in Ref. [59]. As shown in Fig. 6(b), the radius of the KcsA channel is complex in shape, and the selectivity filter is short and narrow with a radius of about 2 Å. The diameter of the cavity in the center of the channel is 10 Å.

The unstructured tetrahedral volume mesh and triangular surface mesh of the KcsA ion channel is shown in Fig. 7. The molecular surface mesh of the KcsA channel was generated using TMSMESH [52], and the number of faces was reduced using ISO2MESH [60]. The program TRANSFORMESH [61] was used to improve the mesh quality. A tetrahedral volume mesh was generated using TETGEN [53]. Finally, the membrane mesh

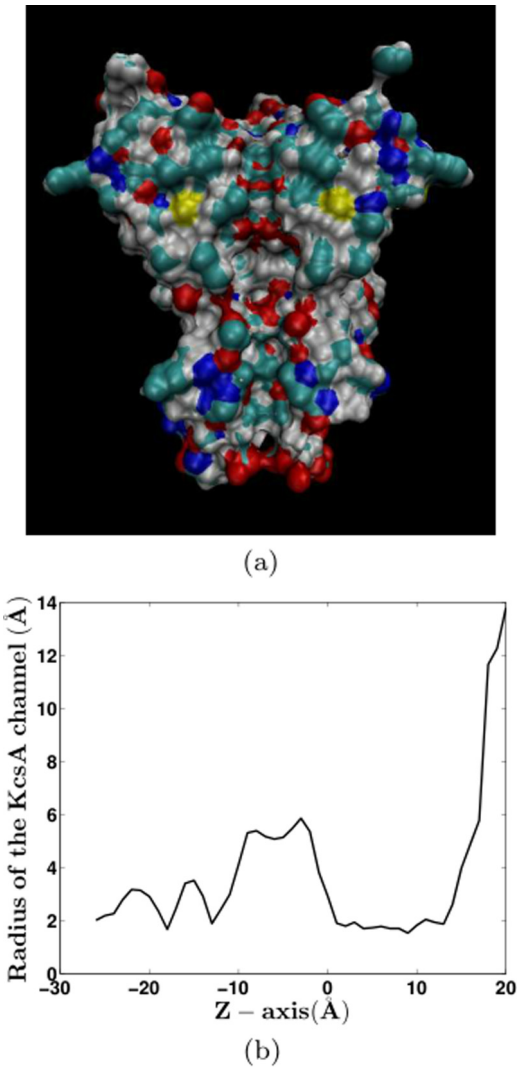

FIG. 6. (a) Molecular surface and (b) pore radius of the KcsA channel (PDB code 1BL8).

was added to the tetrahedral volume mesh, and the boundary faces were properly marked [51]. The mesh over the whole domain has a total of 102 572 vertices and 643 832 tetrahedra.

To study ion selectivity in the KcsA channel using the BPNP model, we considered an electrolyte solution containing two positive ion species (approximately representing Na^+ and K^+) and one negative ion (approximately representing Cl^-). As discussed in Sec. II D, we use the similar position-dependent form for diffusion and dielectric coefficients. The bulk diffusion coefficients are $D^{\mathrm{bulk}}_{\mathrm{Na}} = 0.133$ Å^2/ps, $D^{\mathrm{bulk}}_{\mathrm{K}} = 0.196$ Å^2/ps, and $D^{\mathrm{bulk}}_{\mathrm{Cl}} = 0.203$ Å^2/ps for Na^+, K^+, and Cl^-, respectively. We set $d_1 = 0.1$, $z_0 = 12.5$, and the smoothing parameter $\Delta z = 1.0$. Then the position-dependent diffusion coefficient takes the form

$$D_i(z) = D_i^{\mathrm{bulk}}\left(0.1 + \frac{0.9}{1.0 + e^{-(|z|-12.5)}}\right). \tag{17}$$

For the dielectric coefficient, we set a low dielectric coefficient $\epsilon_c = 30$ in the channel, i.e., the ratio of the effective dielectric coefficient in the channel to that in the bulk region is $\frac{15}{39}$. Then

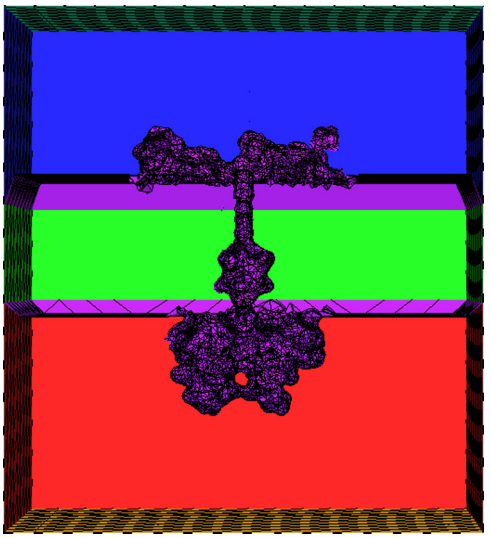

FIG. 7. The unstructured tetrahedral volume mesh and triangular surface mesh of the KcsA ion channel.

the position-dependent dielectric coefficient takes the form

$$\epsilon(z) = 78\left(15/39 + \frac{24/39}{1.0 + e^{-(|z|-12.5)}}\right). \qquad (18)$$

We used the same Born radii ($a_{\mathrm{Na}} = 1.62$ Å, $a_{\mathrm{K}} = 1.95$ Å, and $a_{\mathrm{Cl}} = 2.26$ Å) of these ions as in the simulations of the cylindrical nanopore. We tested some values of the parameter α in Eq. (6). Figure 8 shows the cation concentration changes with the parameter α based on the BPNP model in the KcsA channel under a fixed membrane voltage ($V_0 = -0.20$ V) and bulk concentration ($c^b_{\mathrm{Na}} = 0.1$ M, $c^b_{\mathrm{K}} = 0.1$ M, and $c^b_{\mathrm{Cl}} = 0.2$ M). As shown in Fig. 8, the sodium concentration approaches a very dilute state ($c_{\mathrm{Na}} \sim= 0.005$ M), and the potassium concentration approaches the saturated situation ($c_{\mathrm{K}} \sim= 45$ M) when α is more than 0.25. And there will be some difficulties in obtaining the numerical solution of the BPNP model when α is more than 0.30. It is noted that the parameter α is 0.22 when "saturation" occurs for the above-mentioned

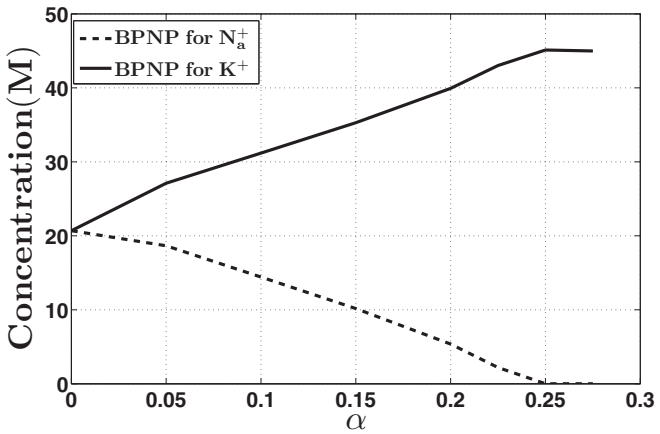

FIG. 8. Cation concentrations in the KcsA channel under a fixed membrane voltage ($V_0 = -0.20$ V) and bulk concentration ($c^b_{\mathrm{Na}} = 0.1$ M, $c^b_{\mathrm{K}} = 0.1$ M, and $c^b_{\mathrm{Cl}} = 0.2$ M) based on BPNP models.

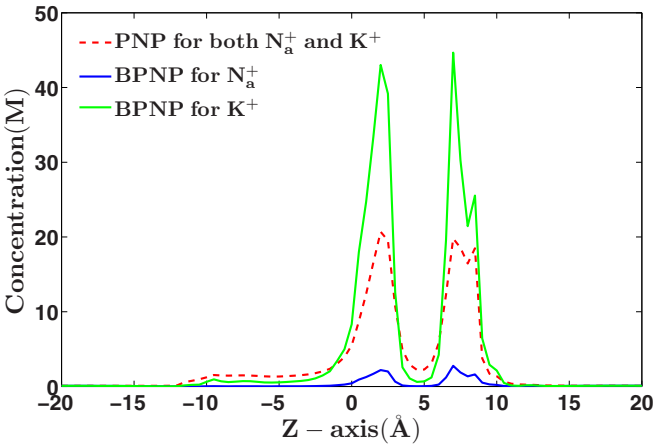

FIG. 9. Cation distributions in the KcsA channel under a fixed membrane voltage ($V_0 = -0.20$ V) and bulk concentration ($c^b_{\mathrm{Na}} = 0.1$ M, $c^b_{\mathrm{K}} = 0.1$ M and $c^b_{\mathrm{Cl}} = 0.2$ M) based on PNP and BPNP models.

nanopore system. In the following simulation studies of KcsA channel, we only took α to 0.225 as an example. The boundary potential at the upper side (extracellular) of the box was also fixed to zero, and that at the bottom side (intracellular) was set from −200 to 200 mV to obtain different membrane potential differences.

We first considered ion distributions in the KcsA channel at different position along the z axis under a fixed membrane voltage ($V_0 = -0.20$ V) and bulk concentration ($c^b_{\mathrm{Na}} = 0.1$ M, $c^b_{\mathrm{K}} = 0.1$ M, and $c^b_{\mathrm{Cl}} = 0.2$ M). Figure 9 demonstrates that the traditional PNP model (the same dashed red lines for both Na^+ and K^+) cannot distinguish between the two cations with the same charge, whereas the BPNP model can clearly distinguish between Na^+ and K^+ ions based on ionic concentration. The distribution of K^+ has two peaks, about 7 Å apart, which is in agreement with the structural property of the two K^+ binding sites presented in Ref. [57]. We calculated the concentrations of cations around the two binding sites. The concentration of K^+ at the positions of either of the two peaks is 43.02 and 44.66 M, respectively, whereas the corresponding concentrations for Na^+ are 2.20 and 2.76 M. This indicates that the BPNP model can clearly predict the selective binding of K^+ over Na^+. However, it is hard to predict that strong selectivity as measured in experiments where K^+ could be 10 000 times more permeant than Na^+ [57]. Similar to the analysis in the previous section, the Born solvation energy will increase when a cation enters the KcsA channel, but the potential barrier will decrease with increasing ion radius. Because K^+ is larger than Na^+, K^+ has a lower potential barrier than Na^+ and can therefore enter the KcsA channel more easily.

The relationship between ionic current and membrane voltage, i.e., the I-V curve, is an important characteristic describing the ion transport property through the channel. The flux can be calculated with Eq. (13). We first considered the potential energy profiles for the KcsA channel. Because the structure of the KcsA channel is highly asymmetric from bottom to top (Fig. 6), the potential energy profiles for membrane voltages 0.20 V (left) and −0.20 V (right) are also not symmetric (Fig. 10). Figure 10 shows electric potential energy profiles (landscape) for PNP and BPNP

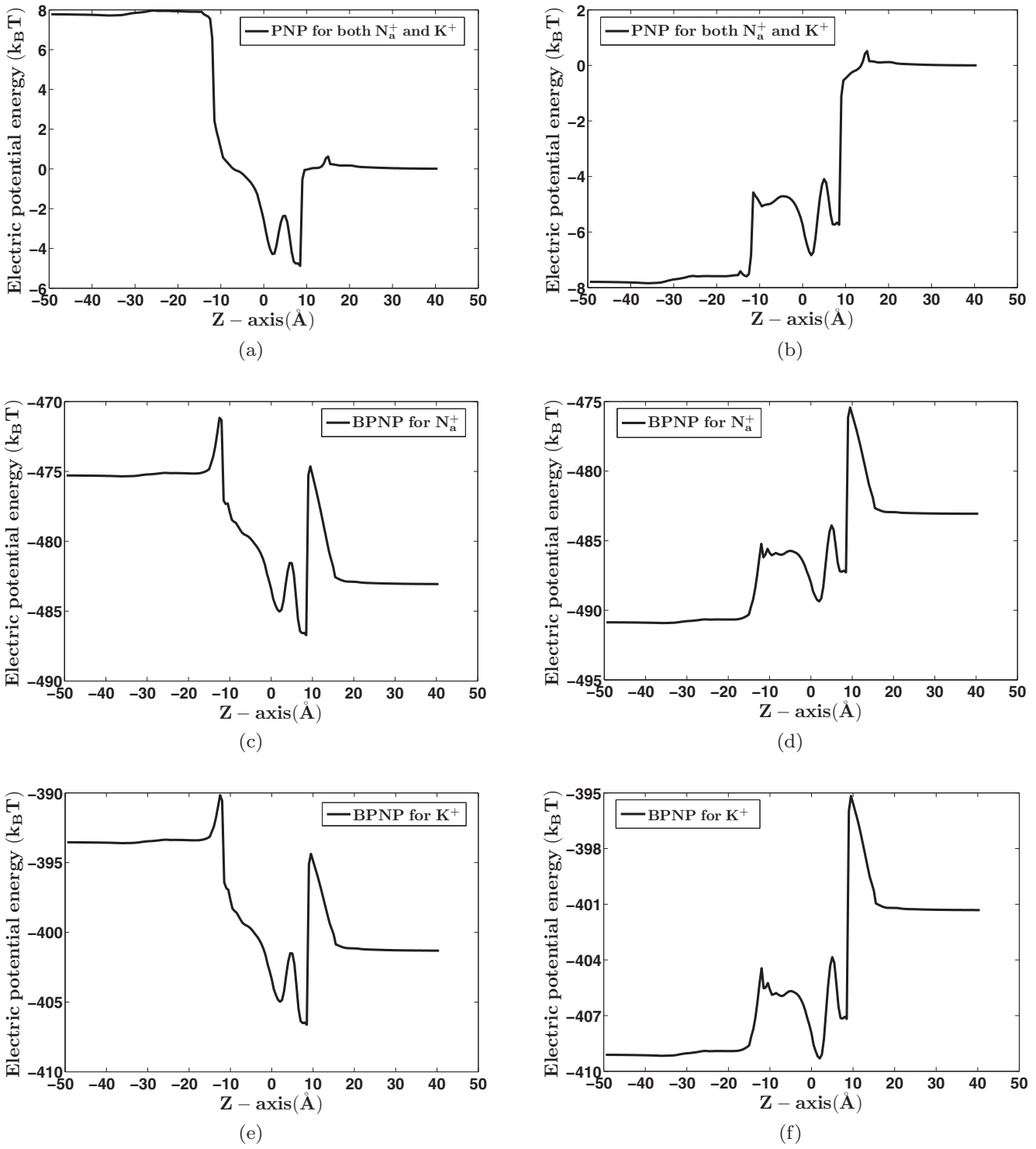

FIG. 10. Electrostatic potential energy profiles (in units of $k_B T$) for the KcsA channel simulated by the PNP and BPNP models with membrane voltages of 0.20 V (left) and −0.20 V (right) in the intracellular region.

models. The electric potential energy of the BPNP model contains electrostatic potential energy and the Born solvation energy:

$$E_{\mathrm{BPNP}} = q_i\phi + \alpha\frac{q_i^2}{2a_i}\left(\frac{1}{\epsilon(r)} - \frac{1}{\epsilon_0}\right), \tag{19}$$

and for the PNP model, the electric potential energy is only the first term ($q_i\phi$). When the cations move from the intracellular to the extracellular region (outward direction), they must overcome a higher potential energy barrier than that when moving from the extracellular to the intracellular region (inward direction) in both models. In the BPNP model, K^+ and Na^+ must overcome almost the same potential barrier ($\sim 11.5 k_B T$) when they move in the outward direction [Figs. 10(c) and 10(e)]. However, K^+ must overcome a lower potential barrier [$\sim 6.0 k_B T$, Fig. 10(f)] than Na^+ [$\sim 7.5 k_B T$,

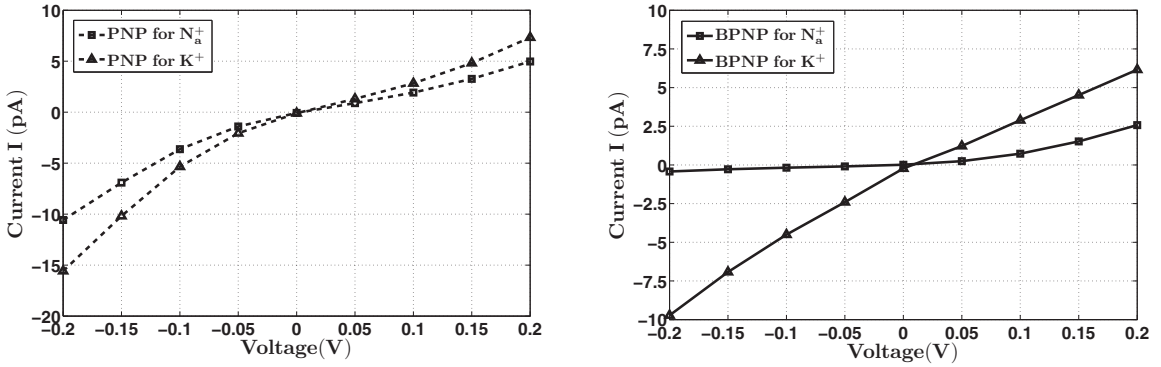

FIG. 11. I-V curves simulated by the (a) PNP and (b) BPNP models for the KcsA channel for bulk concentrations of $c^b_{\mathrm{Na}} = 0.1$ M, $c^b_{\mathrm{K}} = 0.1$ M, and $c^b_{\mathrm{Cl}} = 0.2$ M and membrane voltage differences from -200 to 200 mV.

Fig. 10(d)] when they move in the inward direction. The properties of these energy profiles determine the properties of the I-V curves as discussed in the following.

Figure 11 presents the I-V curves simulated by the PNP and BPNP models for bulk concentrations of $c^b_{\mathrm{Na}} = 0.1$ M, $c^b_{\mathrm{K}} = 0.1$ M, and $c^b_{\mathrm{Cl}} = 0.2$ M and membrane voltage differences from -200 to 200 mV. We considered the rectification ratio $r(\Delta\phi)$, defined as $|I(-\Delta\phi)/I(\Delta\phi)|$, where $\Delta\phi$ is the voltage difference (membrane voltage). The I-V curves simulated by the traditional PNP model [Fig. 11(a)] and the BPNP model [Fig. 11(b)] are asymmetrical [i.e., $|I(-\Delta\phi)| \neq |I(\Delta\phi)|$], which indicates certain so-called rectification effects. However, these two models indicate essentially different rectification effects; see below for a detailed description. And again as expected, PNP results [Fig. 11(a)] do not reflect ion selectivity. The I-V curves of Na^+ and K^+ in the PNP model only have slight differences due to their diffusion coefficients ($D^{\mathrm{bulk}}_{\mathrm{Na}} = 0.133$ and $D^{\mathrm{bulk}}_{\mathrm{K}} = 0.196$ Å^2/ps). As seen in Fig. 11(b), the current of the BPNP model for K^+ is obviously higher than that for Na^+, particularly when the membrane voltage is negative. By comparing the results of PNP [Fig. 11(a)] and BPNP [Fig. 11(b)] models, we found some interesting phenomena. As is common sense, people usually may trivially expect a large ionic current if the concentration in the channel (or binding site) is high. As shown in Fig. 9, the concentration of K^+ in the channel calculated by the BPNP model is significantly higher than that predicted by the traditional PNP model. However, the current for K^+ calculated by the BPNP model is lower than that predicted by the PNP model. As mentioned above, the quantitative relationships between concentration and current are complicated and nonintuitive. As shown in Fig. 11, we also found that the rectification effects for K^+ and Na^+ were different in the BPNP model. Both the PNP and BPNP models simulated ion current rectifications [i.e., $r(\Delta\phi) \neq 1$]. The rectification ratios for both Na^+ and K^+ in the PNP model are about 2, and the ratio for K^+ in the BPNP model is about 1.5, but the rectification ratio for Na^+ in the BPNP model is much smaller than 1 ($\sim 1/6$), which is completely different from that for K^+. This is in contrast to the case of the symmetric cylindrical nanopore, where the I-V curves are symmetric and there is no rectification effect observed (Fig. 5). Therefore, the I-V curves for the KcsA channel show an inward rectifier effect for K^+ and an outward rectifier effect for Na^+, which means K^+ can pass more easily in the inward direction than in the outward direction, i.e., $r(\Delta\phi) > 1$, and the contrary for Na^+. But due to the small current of Na^+, the Na^+ ion almost cannot pass from the extracellular to the intracellular region. This observation agrees with the function of the KcsA potassium channel. These I-V properties are attributed to the asymmetric potential energy landscape originating from the geometry and charge distribution of the channel protein (see Fig. 10).

IV. CONCLUSIONS

We incorporated the Born solvation energy into the mean-field free energy for an inhomogeneous electrolyte with position-dependent dielectric permittivity. We derived a BPNP model based on a variational approach and applied it to study the selective permeation of potassium in a cylindrical nanopore and in a realistic KcsA channel. The BPNP model overcomes the shortcomings of the PNP model by including ion-radius-specific solvation interaction. The BPNP model can differentiate between Na^+ and K^+ ions through simulated ion concentrations and I-V curves. The I-V curves clearly indicate the selectivity of K^+ over Na^+ in the KcsA potassium channel. Both the PNP and BPNP models predicted ion current rectifications in the KcsA channel, but with different results. The I-V curve of the BPNP model for the KcsA channel indicates an inward rectifier effect for K^+ but indicates an outward rectifier effect for Na^+. Future work is to improve the model by incorporating other important factors for ion channels such as the ion volume excluded effect, steric effect, and concentration-dependent dielectric coefficients, and to study channel systems not limited to the potassium channel.

ACKNOWLEDGMENTS

The authors thank our group students Bin Tu and Tiantian Liu for their help. This work was supported by the National Key Research and Development Program of China (Grant No. 2016YFB0201304), the Science Challenge Project (No. TZ2016003), and China NSF (NSFC Grant Nos. 21573274 and 91530102).

[1] D. Boda, D. Henderson, and D. Busath, J. Phys. Chem. B **105**, 11574 (2001).
[2] B. Roux, Annu. Rev. Biophys. Biomol. Struct. **34**, 153 (2005).
[3] M. Valiskó, D. Boda, and D. Gillespie, J. Phys. Chem. C **111**, 15575 (2007).
[4] H. Hwang, G. C. Schatz, and M. A. Ratner, J. Phys. Chem. A **127**, 024706 (2007).
[5] Q. Shao, J. Zhou, L. H. Lu, X. H. Lu, Y. D. Zhu, and S. Y. Jiang, Nano Lett. **9**, 989 (2009).
[6] C. Song and B. Corry, J. Phys. Chem. B **113**, 7642 (2009).
[7] G. W. Wei, Q. Zheng, Z. Chen, and K. L. Xia, SIAM Rev. **54**, 699 (2012).
[8] H. Li, J. S. Francisco, and X. C. Zeng, Proc. Natl. Acad. Sci. U.S.A. **112**, 10851 (2015).
[9] Y. Song, J. H. Lee, H. Hwang, G. C. Schatz, and H. Hwang, J. Phys. Chem. B **120**, 11912 (2016).
[10] J. L. Liu and B. Eisenberg, J. Chem. Phys. **141**, 075102 (2014).
[11] M. Taglialatela and E. Stefani, Proc. Natl. Acad. Sci. U.S.A. **90**, 4758 (1993).
[12] S. Choe, Nat. Rev. Neurosci. **3**, 115 (2002).
[13] Q. F. Zhong, Q. Jiang, P. B. Moore, D. M. Newns, and M. L. Klein, Biophys. J. **74**, 3 (1998).
[14] L. Delemotte, W. Treptow, M. L. Klein, and M. Tarek, Biophys. J. **99**, L72 (2010).
[15] M. Ø. Jensen, V. Jogini, D. W. Borhani, A. E. Leffler, R. O. Dror, and D. E. Shaw, Science **336**, 229 (2012).
[16] J. Ostmeyer, S. Chakrapani, A. C. Pan, E. Perozo, and B. Roux, Nature (London) **501**, 121 (2013).
[17] W. Im, S. Seefeld, and B. Roux, Biophys. J. **79**, 788 (2000).
[18] W. Fu, M. Cui, J. M. Briggs, X. Q. Huang, B. Xiong, Y. M. Zhang, X. M. Luo, J. H. Shen, R. Y. Ji, H. L. Jiang, and K. X. Chen, Biophys. J. **83**, 2370 (2002).
[19] G. Moy, B. Corry, S. Kuyucak, and S. H. Chung, Biophys. J. **78**, 2349 (2000).
[20] B. Corry, S. Kuyucak, and S. H. Chung, Biophys. J. **78**, 2364 (2000).
[21] D. Andreucci, D. Bellaveglia, E. N. M. Cirillo, and S. Marconi, Phys. Rev. E **84**, 021920 (2011).
[22] D. Boda, Annu. Rep. Comput. Chem. **10**, 127 (2014).
[23] R. S. Eisenberg and D. P. Chen, Biophys. J. **64**(2), A22 (1993).
[24] D. Gillespie and R. S. Eisenberg, Eur. Biophys. J. **31**, 454 (2002).
[25] D. Constantin and Z. S. Siwy, Phys. Rev. E **76**, 041202 (2007).
[26] B. Z. Lu, M. J. Holst, J. A. McCammon, and Y. C. Zhou, J. Comput. Phys. **229**, 6979 (2010).
[27] T.-L. Horng, T.-C. Lin, C. Liu, and B. Eisenberg, J. Phys. Chem. B **116**, 11422 (2012).
[28] R. Roth and D. Gillespie, Phys. Rev. Lett. **95**, 247801 (2005).
[29] E. Gouaux and R. MacKinnon, Science **310**, 1461 (2005).
[30] S. Y. Noskov and B. Roux, Biophys. Chem. **124**, 279 (2006).
[31] Y. Qiao, C. Lian, B. Z. Lu, and J. Wu (unpublished).
[32] Y. F. Zhou, J. H. Morais-Cabral, A. Kaufman, and R. MacKinnon, Nature (London) **414**, 43 (2001).
[33] S. Y. Noskov and B. Roux, J. Gen. Physiol. **129**, 135 (2007).
[34] S. Varma, D. Sabo, and S. B. Rempe, J. Mol. Biol. **376**, 13 (2008).
[35] S. Varma, D. M. Rogers, L. R. Pratt, and S. B. Rempe, J. Gen. Physiol. **137**, 479 (2011).
[36] B. Z. Lu and Y. C. Zhou, Biophys. J. **100**, 2475 (2011).
[37] J. L. Liu and B. Eisenberg, J. Phys. Chem. B **117**, 12051 (2013).
[38] Y. Qiao, B. Tu, and B. Z. Lu, J. Chem. Phys. **140**, 174102 (2014).
[39] M. Born, Z. Phys. **1**, 45 (1920).
[40] D. Boda, D. Henderson, B. Eisenberg, and D. Gillespie, J. Chem. Phys. **135**, 064105 (2011).
[41] D. Boda, D. Henderson, and D. Gillespie, J. Chem. Phys. **139**, 055103 (2013).
[42] A. Parsegian, Nature (London) **221**, 844 (1969).
[43] J. P. Dilger, S. G. A. McLaughlin, T. J. McIntosh, and S. A. Simon, Science **206**, 1196 (1979).
[44] X. J. Liu, Y. Qiao, and B. Z. Lu, arXiv:1702.01115, SIAM J. Appl. Math. (to be published).
[45] Y. Z. Wei and S. Sridhar, Rev. Sci. Instrum. **60**, 3041 (1989).
[46] Y. Z. Wei, P. Chiang, and S. Sridhar, J. Chem. Phys. **96**, 4569 (1992).
[47] J. B. Hasted, D. M. Ritson, and C. H. Collie, J. Chem. Phys. **16**, 1 (1948).
[48] B. Hess, C. Holm, and N. van der Vegt, Phys. Rev. Lett. **96**, 147801 (2006).
[49] H. L. Li and B. Z. Lu, J. Chem. Phys. **141**, 024115 (2014).
[50] B. Z. Lu, Y. C. Zhou, M. J. Holst, and J. A. McCammon, Commun. Comput. Phys. **3**, 973 (2008).
[51] B. Tu, M. X. Chen, Y. Xie, L. B. Zhang, B. Eisenberg, and B. Z. Lu, J. Comput. Chem. **34**, 2065 (2013).
[52] M. X. Chen and B. Z. Lu, J. Chem. Theory Comput. **7**, 203 (2011).
[53] H. Si, ACM Trans. Math. Softw. **41**, 1 (2015).
[54] L. B. Zhang, Numer. Math. Theor. Methods. Appl. **2**, 65 (2009).
[55] B. Z. Lu, Y. C. Zhou, G. A. Huber, S. D. Bond, M. J. Holst, and J. A. McCammon, J. Chem. Phys. **127**, 135102 (2007).
[56] Z. S. Siwy, Adv. Funct. Mater. **16**, 735 (2006).
[57] D. A. Doyle, J. M. Cabral, R. A. Pfuetzner, A. Kuo, J. M. Gulbis, S. L. Cohen, B. T. Chait, and R. MacKinnon, Science **280**, 69 (1998).
[58] W. Humphrey, A. Dalke, and K. Schulten, J. Mol. Graphics **14**, 33 (1996).
[59] T. Liu, S. Bai, B. Tu, M. Chen, and B. Lu, Mol. Based Math. Biol. **3**, 128 (2015).
[60] Q. Q. Fang and D. Boas, *in Proceedings of the IEEE International Symposium on Biomedical Imaging: From Nano to Macro Boston*, 2009 (IEEE, New York, 2009), p. 1142.
[61] A. Zaharescu, E. Boyer, and R. P. Horaud, *in Proceedings of the Eighth Asian Conference on Computer Vision Tokyo, 2007* (Springer-Verlag Berlin, Heidelberg, 2007), p. 166.